# Dopants adsorbed as single atoms prevent degradation of catalysts

SANWU WANG[1], ALBINA Y. BORISEVICH*[2], SERGEY N. RASHKEEV[1], MICHAEL V. GLAZOFF[3], KARL SOHLBERG[4], STEPHEN J. PENNYCOOK[1,2] AND SOKRATES T. PANTELIDES[1,2]

[1]Department of Physics and Astronomy, Vanderbilt University, Nashville, Tennessee 37235, USA
[2]Condensed Matter Sciences Division, Oak Ridge National Laboratory, Oak Ridge, Tennessee 37831, USA
[3]Alcoa Technical Center, Alcoa Center, Pennsylvania 15069-0001, USA
[4]Department of Chemistry, Drexel University, Philadelphia, Pennsylvania 19104, USA
*e-mail: albinab@ornl.gov

Published online: 22 February 2004; doi:10.1038/nmat1077

**The design of catalysts with desired chemical and thermal properties is viewed as a grand challenge for scientists and engineers[1]. For operation at high temperatures, stability against structural transformations is a key requirement. Although doping has been found to impede degradation, the lack of atomistic understanding of the pertinent mechanism has hindered optimization. For example, porous $\gamma$-$Al_2O_3$, a widely used catalyst and catalytic support[2–6], transforms to non-porous $\alpha$-$Al_2O_3$ at ~1,100 °C (refs 7–10). Doping with La raises the transformation temperature[8–11] to ~1,250 °C, but it has not been possible to establish if La atoms enter the bulk, adsorb on surfaces as single atoms or clusters, or form surface compounds[10–15]. Here, we use direct imaging by aberration-corrected Z-contrast scanning transmission electron microscopy coupled with extended X-ray absorption fine structure and first-principles calculations to demonstrate that, contrary to expectations, stabilization is achieved by isolated La atoms adsorbed on the surface. Strong binding and mutual repulsion of La atoms effectively pin the surface and inhibit both sintering and the transformation to $\alpha$-$Al_2O_3$. The results provide the first guidelines for the choice of dopants to prevent thermal degradation of catalysts and other porous materials.**

Aberration correction has allowed sub-Ångstrom beams to be formed with huge improvements in the visibility of single atoms[16]. Figure 1a shows a Z-contrast image of a flake of La-doped $\gamma$-$Al_2O_3$ in the [100] orientation. Surprisingly, unlike the undoped case[17,18], there was no apparent preferential exposure of the [110] surface. Instead, the [100] surface was encountered often. The square arrangement of Al–O columns is clearly resolved. In this imaging mode, the intensity contributed by an atom is roughly proportional to $Z^2$, where Z is the atomic number[19], allowing single La atoms to be visible in the form of brighter spots on the background of thicker but considerably lighter $\gamma$-$Al_2O_3$ support. For the average sample thickness, the nominal density (3.5 wt%) corresponds to ~3 La atoms per nm$^2$ in projection. Typical counts of La atoms observed in scanning transmission electron microscopy (STEM) images are consistent with that density. Most of the La atoms are located directly over Al–O columns (site A in Fig. 1a), but a small fraction also occupies a position shifted from the Al–O column (site B in Fig. 1a). Note that in this second configuration, the La atom

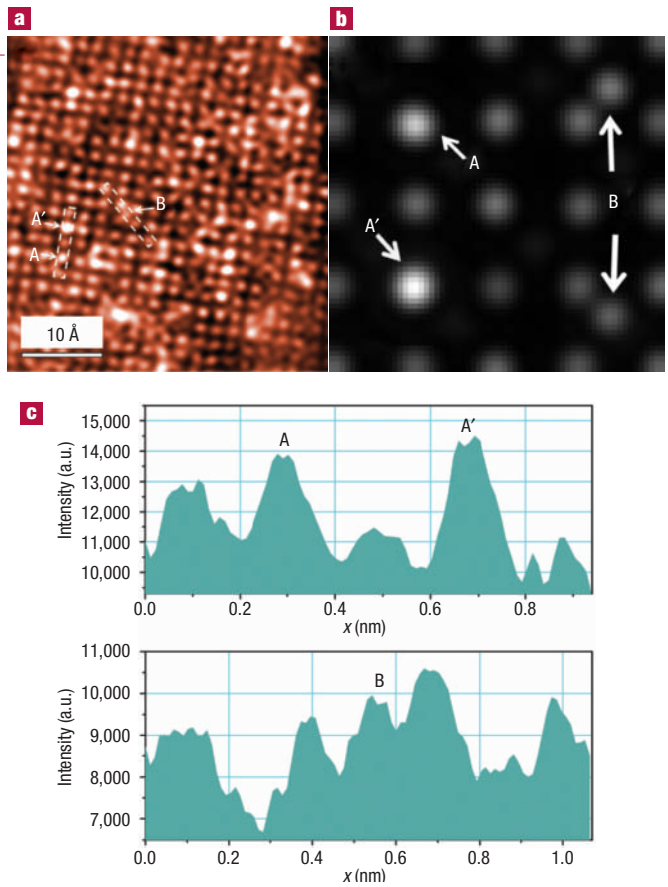


**Figure 1 La atoms on g-$Al_2O_3$ flake in [100] orientation.** **a**, Z-contrast STEM image. Two distinct sites (A(A′) and B) for individual La atoms are seen (images are high- and low-pass filtered). **b**, Multislice simulation[20] of A, A′ and B positions of La atoms over and under a 40-Å slab of $\gamma$-$Al_2O_3$ at zero defocus for an aberration-free probe of 15 mrad semi-angle; one phonon configuration was found sufficient to achieve convergence. **c**, Intensity (in arbitrary units, a.u.) profiles of the smoothed raw data corresponding to the line traces denoted on **a**.

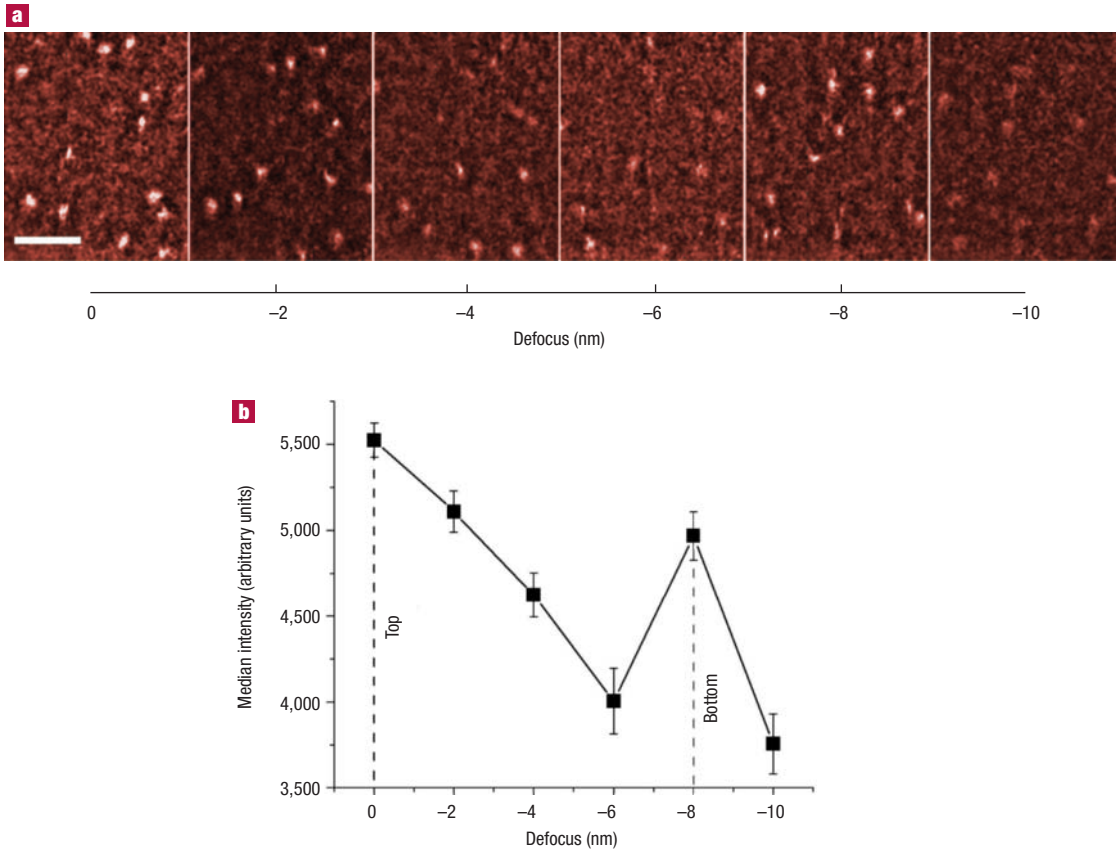


**Figure 2 Depth-sensitive STEM experiment. a**, STEM images (identically processed) taken at different defocus values. Note the intensity peaking at defocus values of 0 and –8 nm. Focus drift did not exceed 0.4 nm from the first to the last frame in the series. Bar length is 1 nm. **b**, Median incremental intensity of the La atom images versus defocus (see Supplementary Information for the original statistical data).

appears much dimmer, because its intensity is no longer superimposed on that of the Al–O column; this effect is also evident in simulated images using multislice codes[20] (Fig. 1b) and in the line traces of the experimental data (Fig. 1c). Furthermore, substitutional La atoms on the beam entrance side of the alumina flake are systematically less bright than those on the exit face (site A′ on Figs 1a–c), where channelling has sharpened the beam; for interstitial La atoms (site B) the intensity difference in the simulated image (Fig. 1b) between the entrance (arrow up) and exit (arrow down) surface is negligible . The images reveal clearly that there is no correlation in the distribution of dopant atoms. The presence of La was also confirmed using electron energy-loss spectra (EELS), acquired over ~100-nm$^2$ areas of the sample. Atomically resolved EELS was not feasible for this material because the necessary prolonged exposure caused significant damage.

Although a Z-contrast image is a two-dimensional (2D) projection of the 3D object, the higher convergence angle of the aberration-corrected STEM probe offers a possibility of depth sensitivity using the decreased depth of focus. Under these conditions, the intensity of an image of a point object (such as single atom) significantly diminishes when it is only nanometres away from the perfect focus. We find that for La-doped $\gamma$-$Al_2O_3$ flakes in the absence of any lattice contrast from the substrate (that is, when it is tilted far off crystallographic axes) two different focus conditions can be identified, which can again be attributed to La atoms located on the top and bottom surface of the flake, respectively. Figure 2a shows an example of such through-focal series of Z-contrast STEM images. It is clear from the figure that the bright spots corresponding to La atoms are sharper at defocus values of 0 and –8 nm, suggesting that the thickness of the examined flake is close to 8 nm. Note that after going past the bottom surface, atoms 'fade' faster, reflecting widening of the probe after passing through the substrate. This conclusion can also be expressed quantitatively as the dependence of median bright spot intensity on defocus (Fig. 2b). This unique experiment demonstrates a depth-sensing capability of the STEM, and corroborates the conclusion that La atoms maintain widely separated surface positions even after high-temperature annealing. Figure 2a also shows that La atoms move relative to one another as the imaging process is repeated with different defocus. Such motion is consistent with the fact that the La atoms reside on the surfaces, where the beam can induce their migration.

Extended X-ray absorption fine structure (EXAFS) measurements were performed on a series of five lanthanum-doped $\gamma$-alumina specimens: a sample without heat treatment (sample 0) and 4 samples annealed at 800, 1,000, 1,200, and 1,400 °C for 3 hours (samples 1–4, respectively). The Fourier transforms of the X-ray absorption spectra recorded at the La $L_{III}$-edge (Fig. 3.) demonstrate that up to 1,200 °C (that is, before the collapse of $\gamma$-$Al_2O_3$ structure) no noticeable changes occur in the coordination of La. Simulations of the EXAFS spectra differ markedly from the observed spectra if one or more La atoms are inserted in the first or second coordination shells of La, indicating that adsorbed La atoms are isolated, in agreement with the conclusion reached from the Z-contrast images. An excellent fit is obtained for sample 4 by using twelve oxygen atoms in the first coordination shell and six aluminium

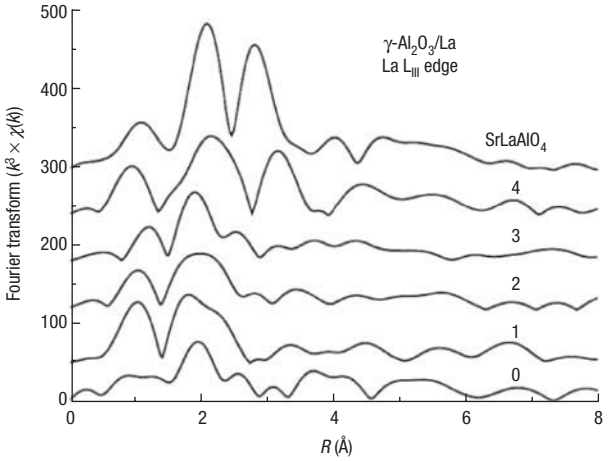


**Figure 3 Fourier transforms (into direct space) of the synchrotron EXAFS La $L_{III}$-edge spectra $\chi(k)$ (where $k$ is the wave vector) of La/γ-$Al_2O_3$ samples ($R$ denotes distance from La atom).** Sample 0 without heat treatment, and samples 1–4 annealed at 800, 1,000, 1,200, and 1,400 °C, respectively. Note that no changes in the spectra occur before 1,400 °C. The peaks below 1.5 Å are artefacts arising from a Fourier transform on a finite domain.

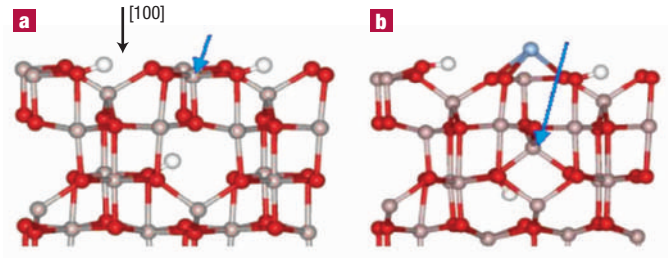


**Figure 4 Configurations for the (100) surface of γ-$Al_2O_3$, determined by first-principles calculations. a**, undoped, and **b**, La-doped. The Al, O, H and La atoms are shown in grey, red, white, and blue, respectively. The position of the aluminium atom that relaxes from the surface into the cation vacancy is indicated by the blue arrow.

atoms in the second shell, suggesting an ordered bulk phase. Simulation of the spectra from samples 0–3 show that the peak at ~3 Å of sample 4 can be suppressed by decreasing the number of oxygen atoms in the first shell from twelve to less than eight, and distributing La–O distances, suggesting surface-like environment. The significant change in the local coordination of the La occurring at 1,400 °C (sample 4) can be attributed to the γ–α phase transition. The exact form of La after the transition has not yet been identified.

Figure 4 represents the minimum energy configurations of the undoped and La-doped (100) surface obtained from first-principles calculations. In the absence of La, the (100) surface (Fig. 4a) shows only minor relaxation effects; all the surface aluminium atoms are five-coordinated and the surface oxygen atoms are either three- or four-coordinated. The cation vacancies are located between the first and second oxygen subsurface layer. However, when a La atom is introduced, a significant relaxation of the structure occurs. One of the five-coordinated Al atoms (adjacent to La) is displaced from the surface into the subsurface tetrahedral vacancy site (Fig. 4b). The La atom occupies the resultant surface fourfold hollow site, which is close to the initial location of the Al atom in planar coordinates but located ~1.2 Å above it, making La–O bond lengths 2.3–2.5 Å. This configuration, obtained independently by total-energy minimization, is precisely the same as site A on the micrograph in Fig. 1a. Calculations aimed at revealing the structure of the observed B site found that it corresponds to a La atom with one of the four neighbouring surface oxygen atoms missing. The asymmetry forces the La atom off the Al–O column, as observed. Its formation is clearly the result of the presence of surface oxygen vacancies.

Additional calculations exploring the incorporation of La atoms in bulk γ-$Al_2O_3$ found that a La atom, when initially placed at a vacancy, interstitial, or substitutional site in the second or third subsurface layer, would relax up to the surface. When a La atom is initially located in a deeper layer (the 8th or 9th layer of the supercell for the (100) surface, and the 5th or 6th layer for the (110C) surface), which is equivalent to the bulk, the total energy of the system is significantly higher than that of the configuration with La on the surface (models with La in different bulk sites were examined). The preference for surface sites over the bulk arises primarily from the strong binding of La on the surface and the large difference in ionic size between $La^{+3}$ (1.03 Å) and $Al^{+3}$ (0.54 Å)[21]. The theoretical result corroborates the through-focus imaging analysis of Fig. 2. The marked preference for surface sites versus the bulk is an important factor in the inhibition of sintering. Progress of the sintering process would inevitably trap some of the surface La atoms in the bulk, thus forcing the system into highly strained and energetically unfavourable configuration. The resulting inhibition effect helps retain a large specific surface area for γ-$Al_2O_3$ at higher temperatures, in agreement with experimental observations[9–11,22].

The binding energy of La to the (100) surface is very high (8.6 eV), due partly to the removal of the surface Al atom into the subsurface, which enhances the attractive interaction between La and the surface oxygen atoms and reduces the otherwise strong repulsion between La and the Al atom. The strong binding also causes large migration energies (4–5 eV) for typical paths connecting equivalent configurations. Similar calculations for the (110C) surface, which is exposed preferentially in the undoped γ-$Al_2O_3$ (refs 17,18), also resulted in high values of the binding energy (7.5 eV). In this case, however, La atoms occupy existing surface hollow sites, which are created on the undoped surface[18,23] by displacement of three-coordinated surface Al atoms into the empty octahedral sites in the first subsurface layer. The difference in the two binding energies explains the occurrence of (100) surfaces after annealing in the presence of La dopant. When the same computational procedure is carried out for the α-$Al_2O_3$ (0001) surface, much lower binding energy (4.3 eV) for La atoms is obtained. This difference means that doping would cause an increase in the enthalpy of α-$Al_2O_3$ relative to γ-$Al_2O_3$, thus further stabilizing γ-$Al_2O_3$.

Stabilization of γ-$Al_2O_3$ by La is often suggested to be due to $LaAlO_3$ or $La_2O_3$ monolayers on the surface, and the debate about the formation of one phase over another is still ongoing[10–15]. We explored the possibility of clustering of surface La atoms. When placed in the nearest interstitials above the (110C) surface of γ-$Al_2O_3$, two La atoms do not show any tendency to create any bond between them. Instead, they move away from each other when the initial distance between them is less than 4 Å, thus suggesting that there is no driving force for the formation of dopant clusters or monolayers, unlike previously proposed models[12–15] and in complete agreement with our images. This effect suggests that the sintering can be effectively inhibited by a very small amount of La dopant, provided that atomically dispersed distribution can be achieved by a given preparation method; indeed laboratory experiments demonstrate that stabilization can be achieved with only 0.3 wt% of dopant versus the usual 3–5% (ref. 10).

To summarize, we have used a combination of experimental and theoretical results to elucidate the role of La impurities in the stabilization of $\gamma$-$Al_2O_3$ to high temperatures. The three methods yield complementary information that leads to a single overriding conclusion: La atoms eschew the bulk and adsorb strongly on $\gamma$-$Al_2O_3$ surfaces as isolated atoms, strongly pinning the surface and impeding sintering and phase transformation to avoid getting trapped in the bulk of $\gamma$-$Al_2O_3$ or the surface of $\alpha$-$Al_2O_3$. These results can be used as guidelines in the choice of dopants for other systems where thermal stability is important.

## METHODS

Samples were prepared using commercial material, Alcoa product Ga-200L, which is $\gamma$-$Al_2O_3$ stabilized with La (3.5 wt% of $La_2O_3$). The samples for the STEM study were annealed at 1,000 °C for 10 hours, which produced higher crystallinity, facilitating Z-contrast imaging.

Z-contrast STEM observations were made with VG Microscopes HB603U (East Grinstead, UK) operated at 300 kV and equipped with a Nion (Kirkland, Washington, USA) aberration corrector to give a probe size of 0.7–0.8 Å and superior signal-to-noise ratio[24].

EXAFS measurements were performed in the regime of total external reflection at room temperature at the Institute of Nuclear Physics of the Russian Academy of Sciences (the Novosibirsk Center for Synchrotron Radiation). Synchrotron radiation was properly pre-conditioned using the Si (111) monochromator. FEFF5 software was used for EXAFS data analysis.

The first-principles calculations were performed within density functional theory, using the pseudopotential method and a plane-wave basis set[25]. Exchange correlation was included using the generalized gradient-corrected functionals (GGA) given by Perdew and Becke[26,27]. We adopted the Vanderbilt ultrasoft pseudopotentials for oxygen and hydrogen atoms, a norm-conserving pseudopotential for Al, and a projector augmented wave (PAW) potential for La (refs 28–30). A plane-wave energy cut-off of 400 eV and two special *k* points in the irreducible part of the 2D Brillouin zone of the surfaces were used for calculating both the (100) and (110) surfaces of γ-Al2O3. Semi-infinite (100) and (110) surfaces were modelled by repeated slabs (supercells) containing 7–12 atomic layers for the (100) surface and 5–8 layers for the (110) surface (68–112 and 70–128 atoms, respectively) separated by a vacuum region equivalent to 10–12 Å (supercells containing 80 atoms and a 2 × 2 surface cell were used to represent the $\alpha$-$Al_2O_3$ surface). The cation vacancies that are inherently present in the spinel form of $\gamma$-$Al_2O_3$ were located on the tetrahedral cation sublattice. All the atoms in the supercell except for those in the lower one or two atomic layers (which were kept fixed) were relaxed until the forces on the atoms were smaller than 0.05 eV $Å^{-1}$.

Received 15 October 2003; accepted 19 January 2004; published 22 February 2004.

## References


1. Bell, A. T. The impact of nanoscience on heterogeneous catalysis. *Science* **299,** 1688–1691 (2003).
2. Satterfield, C. N. *Heterogeneous Catalysis in Practice* (McGraw Hill, New York, 1980).
3. Knozinger, H. & Ratnasamy, P. Catalytic aluminas – surface models and characterization of the surface sites. *Catal. Rev. Sci. Eng.* **17,** 31–69 (1978).
4. Gates, B. C. Supported metal clusters: synthesis, structure, and catalysis. *Chem. Rev.* **95,** 511–522 (1995).
5. Xu, Z. *et al.* Size-dependent catalytic activity of supported metal clusters. *Nature* **372,** 346–8 (1994).
6. Lin, V. S. Y. *et al.* Oxidative polymerization of 1,4-diethynylbenzene into highly conjugated poly(phenylene butadiynylene) within the channels of surface-functionalized mesoporous silica and alumina materials. *J. Am. Chem. Soc.* **124,** 9040–9041 (2002).
7. Wefers, K. & Misra, C. Oxides and hydroxides of aluminum. (Alcoa Technical Paper No.19, Alcoa Laboratories, Pittsburgh, 1987).
8. Arai, H. & Machida, M. Thermal stabilization of catalyst supports and their application to high-temperature catalytic combustion. *Appl. Catal. A* **138,** 161–176 (1996).
9. Church, J. S., Cant, N. W. & Trimm, D. L. Surface area stability and characterization of a novel sulfate-based alumina modified by rare earth and alkaline earth ions. *Appl. Catal. A* **107,** 267–276 (1994).
10. Glazov, M. V., Novak, J. & Hector, L. G. Stabilization of γ-alumina: how much lanthanum do we actually need? (Alcoa Technical Paper No. 99–168, Alcoa Technical Center, Pittsburgh, 1999).
11. Kumar, K. –N. P., Tranto, J., Kumar, J. & Engell, J. E. Pore-structure stability and phase transformation in pure and M-doped (M = La, Ce, Nd, Gd, Cu, Fe) alumina membranes and catalyst supports. *J. Mater. Sci. Lett.* **15,** 266–270 (1996).
12. Oudet, F., Courtine, P. & Vieux, A. Thermal stabilization of transition alumina by structural coherence with lanthanide aluminum oxide ($LnAlO_3$, Ln = lanthanum, praseodymium, neodymium). *J. Catal.* **114,** 112–120 (1988).
13. Beguin, B., Garbowski, E. & Primet, M. Stabilization of alumina by addition of lanthanum. *Appl. Catal.* **75,** 119–132 (1991).
14. Vazquez, A. *et al.* X-ray diffraction, FTIR, and NMR characterization of sol–gel alumina doped with lanthanum and cerium. *J. Solid State Chem.* **128,** 161–168 (1997).
15. Yamamoto, T., Tanaka, T., Matsuyama, T., Funabiki, T. & Yoshida, S. Structural analysis of La/$Al_2O_3$ catalysts by La K-edge XAFS. *J. Synchrotron Rad.* **8,** 634–636 (2001).
16. Batson, P. E., Dellby, N. & Krivanek, O. L. Sub-ångstrom resolution using aberration corrected electron optics. *Nature* **418,** 617–620 (2002).
17. Blonski, S. & Garofalini, S. H. Molecular dynamics simulations of γ-alumina and α-alumina surfaces. *Surf. Sci.* **295,** 263–274 (1993).
18. Sohlberg, K., Pennycook, S. J. & Pantelides, S. T. Explanation of the observed dearth of three-coordinated Al on γ-alumina surfaces. *J. Am. Chem. Soc.* **121,** 10999–11001 (1999).
19. Pennycook, S. J. & Jesson, D. E. High-resolution incoherent imaging of crystals. *Phys. Rev. Lett.* **64,** 938–941 (1990).
20. Kirkland, E. J. *Advanced Computing in Electron Microscopy* (Plenum, New York, 1998).
21. Shannon, R. D. Revised effective ionic radii and systematic studies of interatomic distances in halides and chalcogenides. *Acta Cryst. A* **32,** 751–767 (1976).
22. Burtin, P., Brunelle, J. P., Pijolat, M. & Soustelle, M. Influence of surface area and additives on the thermal stability of transition alumina catalyst supports. I. Kinetic data. *Appl. Catal.* **34,** 225–238 (1987).
23. Rashkeev, S. N. *et al.* Transition metal atoms on different alumina phases: The role of subsurface sites on catalytic activity. *Phys. Rev. B* **67,** 115414 (2003).
24. Krivanek, O. L., Dellby, N. & Lupini, A. R. Towards sub-Å electron beams. *Ultramicroscopy* **78,** 1–11 (1999).
25. Kresse, G. & Furthmüller, J. Efficiency of ab-initio total energy calculations for metals and semiconductors using a plane-wave basis set. *Comput. Mater. Sci.* **6,** 15–50 (1996).
26. Perdew, J. P. Density-functional approximation for the correlation energy of the inhomogeneous electron gas. *Phys. Rev. B* **33,** 8822–8824 (1986).
27. Becke, A. D. Density-functional exchange-energy approximation with correct asymptotic behavior. *Phys. Rev. A* **38,** 3098–3100 (1988).
28. Vanderbilt, D. Soft self-consistent pseudopotentials in a generalized eigenvalue formalism. *Phys. Rev. B* **41,** 7892–7895 (1990).
29. Blöchl, P. E. Projector augmented-wave method. *Phys. Rev. B* **50,** 17953–17979 (1994).
30. Kresse, G. & Joubert, D. From ultrasoft pseudopotentials to the projector augmented-wave method. *Phys. Rev. B* **59,** 1758–1775 (1999).


## Acknowledgements

We thank Valeria V. Vavilova and Yanzhao Cao for their help and John W. Novak, Jr for his support. Access to the Novosibirsk Synchrotron Facility (Russian Academy of Sciences) and to the Florida State University supercomputers (csit1 and csit2) are also gratefully acknowledged. This work was supported in part by National Science Foundation Grant DMR-0111841, Department of Energy Grant at Drexel University DE-FC02-01CH11085, by the William A. and Nancy F. McMinn Endowment at Vanderbilt University, by the Division of Materials Sciences, by Laboratory Directed R&D Program for the US Department of Energy, under contract DE-AC05-00OR22725 managed by UT-Battelle, and by an appointment to ORNL Postdoctoral Research Program administered jointly by ORNL and Oak Ridge Institute for Science and Education (ORISE).

Correspondence and requests for materials should be addressed to A.Y.B.

Supplementary Information accompanies the paper on www.nature.com/naturematerials

## Competing financial interests

The authors declare that they have no competing financial interests.